

# Multiple electron-hole scattering effect on quasiparticle properties in a homogeneous electron gas

I. A. Nechaev<sup>1,\*</sup> and E. V. Chulkov<sup>1,2</sup>

<sup>1</sup>*Donostia International Physics Center (DIPC),*

*P. de Manuel Lardizabal 4, 20018, San Sebastián, Basque Country, Spain*

<sup>2</sup>*Departamento de Física de Materiales, Facultad de Ciencias Químicas,*

*UPV/EHU and Centro Mixto CSIC-UPV/EHU, Apdo. 1072, 20080 San Sebastián, Basque Country, Spain*

(Dated: November 21, 2018)

We present a detailed study of a contribution of the  $T$  matrix accounting for multiple scattering between an electron and a hole to the quasiparticle self-energy. This contribution is considered as an additional term to the  $GW$  self-energy. The study is based on a variational solution of the  $T$ -matrix integral equation within a local approximation. A key quantity of such a solution, the local electron-hole interaction, is obtained at the small four-momentum transfer limit. Performed by making use of this limit form, extensive calculations of quasiparticle properties in the homogeneous electron gas over a broad range of electron densities are reported. We carry out an analysis of how the  $T$ -matrix contribution affects the quasiparticle damping rate, the quasiparticle energy, the renormalization constant, and the effective mass enhancement. We find that in comparison with the  $GW$  approximation the inclusion of the  $T$  matrix leads to an essential increase of the damping rate, a slight reduction of the  $GW$  band narrowing, a decrease of the renormalization constant at the Fermi wave vector, and some “weighting” of quasiparticles at the Fermi surface.

PACS numbers: 71.10.-w

## I. INTRODUCTION

It is well known that the extensively used  $GW$  approximation (GWA) to the quasiparticle self-energy is one of the most successful methods for describing the quasiparticle properties in a broad spectrum of materials.<sup>1,2,3,4</sup> This approximation employs only the first term in the Hedin self-energy diagrammatic expansion<sup>5</sup> in the dynamically screened Coulomb interaction (or the so-called *test charge*—*test charge* screened interaction). However, in a number of cases, for example, ferromagnetic transition metals,<sup>6</sup> the GWA is less satisfactory. It requires the cases to go beyond the GWA (see, e.g., Refs. 7,8,9).

One of the approximations that allows one to relatively simply go beyond the GWA is the so-called  $GW\Lambda$  approximation ( $\Lambda$  stands for the three-point vertex function). The latter includes vertex corrections to the  $GW$  self-energy in the same way as it can be done for the irreducible polarizability by means of the spin-symmetric local-field factor. Thus the  $GW\Lambda$  approximation, as well as the GWA, accounts for charge-density fluctuations only. Moreover, this approximation depends weakly on the local-field factor and gives results close to those in the GWA (see Refs. 10 and 11). Note that it can be considered as a  $GW$ -like approximation, where the  $GW$  formula for the quasiparticle self-energy is used but with the *electron*—*test charge* screened interaction instead of the *test charge*—*test charge* one.

The  $GW$  formula for the self-energy can also be derived in approximations using the exact Ward identity as a starting point (see, e.g., Ref. 12). In this case, the role of the screened interaction  $W$  is played by the effective *electron*—*electron* screened interaction that includes the local-field effects by means of the spin-symmetric and

spin-asymmetric local-field factors and, thereby, takes into account the contributions of both charge and spin fluctuations (see also Refs. 13,14,15,16, and references therein).

The specific feature of the approaches mentioned above is the use of the local-field factors which are defined outside the scope of these approaches and, as a rule, are tabulated and parametrized by using quantum Monte Carlo (QMC) calculations for the homogeneous electron gas. It causes certain difficulties in the description of quasiparticle properties, since these factors do not include real system band structure effects. Thus, it is important to find a feasible and all-sufficient scheme for approximate calculations of the self-energy which would allow us to preserve the advantages of the GWA and at that to give a possibility of an inclusion of both charge- and spin-density fluctuations, that is crucial<sup>16,17,18</sup> to obtain agreement with experimental data.

In the preceding paper,<sup>19</sup> hereafter referred to as I, we have examined a possibility to go beyond the GWA by summing an infinite number of ladder diagrams of the Hedin self-energy expansion. To this end, we have found a variational solution of the Bethe-Salpeter equation (more precisely the ladder approximation to this equation<sup>20</sup>) determining the four-point  $T$  matrix that describes multiple scattering of propagating particles. The solution has been obtained within a local approximation in the spirit of Refs. 12 and 21. Making use of this solution, we have proposed a form for the quasiparticle self-energy which allows one to take into account charge- and spin-density fluctuations without double counting. A key quantity of such an approach is the local interaction  $\tilde{W}$ . In fact, the sum of the ladder diagrams is reduced to this interaction just as vertex corrections to

the random phase approximation (RPA) polarizability can be reduced to the spin-symmetric local-field factor (see, e.g., Refs. 21,22,23,24,25). However, the point is that the interaction  $\tilde{W}$  is defined by an eightfold integral and as such is problematical to be realized in *ab initio* calculations for real systems.

Thus, the goal of this paper is twofold. Having restricted ourselves to the multiple electron-hole scattering case, first, we find an expression for  $\tilde{W}$  suitable for *ab initio* calculations. As we are mainly interested in small quasiparticle excitation energy, we consider the small four-momentum transfer limit for this interaction. Second, making use of the obtained limit form of  $\tilde{W}$ , we analyze what effect the  $T$ -matrix contribution being an additional term to the  $GW$  self energy has on quasiparticle properties determined by both the self-energy and its derivatives with respect to momentum and frequency. In this paper, we examine the  $T$ -matrix contribution as applied to the homogeneous electron gas in the paramagnetic state.

The paper is organized as follows. In Sec. II, we derive explicit expressions for the spin-diagonal and spin-non-diagonal parts of the local electron-hole interaction at the small four-momentum transfer limit. Within the model of the homogeneous electron gas in the paramagnetic state, by making use of the connection between the local interaction and the exchange part of the local-field factor, we examine these expressions by comparing with the results known from the literature. In Sec. III we present our main results of extensive calculations carried out for quasiparticle properties over a broad range of electron densities (for  $r_s$  values ranging from 2 to 56). On the base of these results, we analyze how the  $T$ -matrix inclusion with the obtained limit form for the local interaction modifies quasiparticle properties evaluated from the  $GW$  calculations. Finally, the conclusions are given in Sec. IV. Unless stated otherwise, atomic units are used throughout, i.e.,  $e^2 = \hbar = m = 1$ .

## II. LADDER APPROXIMATION

In this section, we derive basic expressions defining the local electron-hole interaction at the small four-momentum transfer limit. Using the relation between this interaction and the exchange part of the local-field factor, we compare our results for the homogeneous electron gas (HEG) with those existing in the literature.

### A. $T$ matrix

The  $T$  matrix shown in Fig. 1(a) allows one to treat the problem of summation of infinite classes of ladder diagrams in the diagrammatic expansion of both the irreducible polarizability [Fig. 1(b)] and the quasiparticle self-energy [Fig. 1(c)]. In momentum space, within the

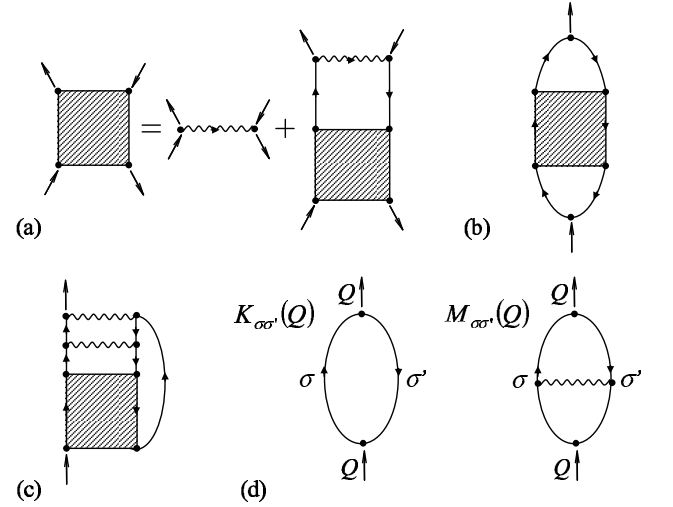


FIG. 1: A diagrammatic representation of the  $T$  matrix (a), accounting for multiple electron-hole scattering, the considered ladder diagrams for the irreducible polarizability  $P$  (b), and the  $T$ -matrix contribution  $\Sigma^T$  to the self-energy (c). (d) Feynman diagrams for  $K_{\sigma\sigma'}(Q)$  and  $M_{\sigma\sigma'}(Q)$ . The wiggly lines signify the dynamically screened Coulomb interaction  $W$ . The solid lines with arrows represent the Green function  $G$ . The  $T$  matrix is shown by the shaded square.

local approximation the  $T$  matrix accounting for multiple electron-hole ( $e - h$ ) scattering has the form<sup>19</sup>

$$\tilde{\Gamma}_{\sigma\sigma'}(Q) = \frac{\tilde{W}_{\sigma\sigma'}(Q)}{1 - \tilde{W}_{\sigma\sigma'}(Q)K_{\sigma\sigma'}(Q)}. \quad (1)$$

Here and in the following we use the four-momentum variables  $Q$ ,  $k$ , or  $p$  as a shorthand for  $(\mathbf{Q}, \Omega)$ ,  $(\mathbf{k}, \omega)$ , or  $(\mathbf{p}, \bar{\omega})$ , respectively.  $\sigma$  labels the spin, and  $\sigma = \pm$  corresponds to spin-up, and spin-down, respectively. The  $e - h$  propagator  $K_{\sigma\sigma'}$  is given by<sup>26</sup>

$$K_{\sigma\sigma'}(Q) = \int dp \kappa_{\sigma\sigma',Q}(p), \quad (2)$$

$$\kappa_{\sigma\sigma',Q}(p) = \frac{i}{(2\pi)^4} G_\sigma(Q + p) G_{\sigma'}(p), \quad (3)$$

where  $G_\sigma$  is the Green function. The local electron-hole interaction  $\tilde{W}_{\sigma\sigma'}$  is related with the dynamically screened Coulomb interaction  $W$  by the equation [see Fig. 1(d)]

$$\tilde{W}_{\sigma\sigma'}(Q) = [K_{\sigma\sigma'}(Q)]^{-1} M_{\sigma\sigma'}(Q) [K_{\sigma\sigma'}(Q)]^{-1}, \quad (4)$$

where

$$M_{\sigma\sigma'}(Q) = \int dk dp \kappa_{\sigma\sigma',Q}(k) W(k - p) \kappa_{\sigma\sigma',Q}(p). \quad (5)$$

Note that the  $T$  matrix (1) depends only on the four-momentum transfer along the electron-hole channel.

In spite of this simple form, a calculation of the  $T$  matrix for the real system is still difficult due to the eight-fold integration in Eq. (5) defining the local interaction.

In this paper, in order to obtain a suitable expression for  $\widetilde{W}_{\sigma\sigma'}$ , we consider the small four-momentum transfer limit (i.e., we set  $\Omega = 0$  and then take the limit  $\mathbf{Q} \rightarrow 0$ ). It is expected to be a reasonable approximation because we are mainly interested in excitations in the vicinity of the Fermi energy where quasiparticles are well defined.

## B. Local interaction

First of all we examine the spin-diagonal part of the local interaction. Omitting arguments which one can find in Ref. 27, in the calculation of poles contribution to the integral (5) we replace  $\kappa_{\sigma\sigma,Q}(k)$  by  $C_{\sigma\sigma}\delta(\omega)\delta[\epsilon_{\sigma}(\mathbf{k})]$ . Unless stated otherwise, the quasiparticle energy  $\epsilon_{\sigma}(\mathbf{k})$  is measured from the Fermi energy  $\epsilon_F$ . The coefficient  $C_{\sigma\sigma}$  is determined by the relation (2). Thus,  $\kappa_{\sigma\sigma,Q}(k)$  can be written as

$$\kappa_{\sigma\sigma,Q}(k) = \frac{1}{8\pi^3 N_F^{\sigma}} K_{\sigma\sigma}(Q) \delta(\omega) \delta[\epsilon_{\sigma}(\mathbf{k})] + \varphi(k), \quad (6)$$

where  $\varphi(k)$  is the regular part of  $\kappa_{\sigma\sigma,Q}(k)$  and  $N_F^{\sigma}$  is the density of states of spin  $\sigma$  per unit volume at the Fermi surface.<sup>28</sup> Substituting Eq. (6) into Eq. (5) and neglecting<sup>29</sup> terms with  $\varphi$ , we obtain that at the considered limit the local interaction has the form

$$\widetilde{W}_{\sigma\sigma} = \frac{\int d\mathbf{k} d\mathbf{p} \delta[\epsilon_{\sigma}(\mathbf{k})] W(\mathbf{k} - \mathbf{p}, 0) \delta[\epsilon_{\sigma}(\mathbf{p})]}{[8\pi^3 N_F^{\sigma}]^2} \quad (7)$$

or

$$\widetilde{W}_{\sigma\sigma} = \frac{1}{[8\pi^3 N_F^{\sigma}]^2} \int_{S_F^{\sigma}} \frac{dS_{\mathbf{k}}}{|\mathbf{v}_{\sigma}(\mathbf{k})|} W(\mathbf{k} - \mathbf{p}, 0) \frac{dS_{\mathbf{p}}}{|\mathbf{v}_{\sigma}(\mathbf{p})|}, \quad (8)$$

where  $S_F^{\sigma}$  is the Fermi surface for spin  $\sigma$ , and  $\mathbf{v}_{\sigma}(\mathbf{k}) = \nabla_{\mathbf{k}}\epsilon_{\sigma}(\mathbf{k})$  is the quasiparticle velocity at this surface. Now we have the fourfold integration instead of the eightfold one in Eq. (5).

For the HEG in the spin-polarized state, Eq. (8) can be rewritten as

$$\widetilde{W}_{\sigma\sigma} = \frac{1}{(4\pi)^2} \int d\Omega_{\mathbf{k}} d\Omega_{\mathbf{p}} W(k_F^{\sigma} |\hat{\mathbf{k}} - \hat{\mathbf{p}}|, 0), \quad (9)$$

where  $\Omega_{\mathbf{k}}$  and  $\Omega_{\mathbf{p}}$  are spatial angles,  $\hat{\mathbf{k}}$  and  $\hat{\mathbf{p}}$  are unit vectors. The Fermi wave vector  $k_F^{\sigma}$  for spin  $\sigma$  is related to that in the paramagnetic state  $k_F$  by  $k_F^{\sigma} = k_F(1 - \sigma\zeta)^{1/3}$ , where the relative spin polarization  $\zeta = |n_+ - n_-|/n$  ( $n_{\sigma}$  is the spin  $\sigma$  electron density,  $n = n_+ + n_-$  being the HEG electron density) defines the exchange splitting of the band as  $2\Delta = \frac{k_F^2}{2} [(1 + \zeta)^{2/3} - (1 - \zeta)^{2/3}]$ .<sup>30</sup> Note that considering the HEG, here and in the following, in all expressions we use the noninteracting energy  $\epsilon_{\sigma}^0(\mathbf{k}) = \mathbf{k}^2/2 - k_F^{\sigma 2}/2$  in place of  $\epsilon_{\sigma}(\mathbf{k})$ , but for the quasiparticle energy in this case the notation  $E_k$  is used (see Sec. III B).

As to the spin-non-diagonal part of the local interaction, instead of  $\delta[\epsilon_{\sigma}(\mathbf{k})]$  in the expression replacing

$\kappa_{\sigma - \sigma, Q}(k)$  we can use the ratio

$$\gamma_{\sigma - \sigma}(\mathbf{k}) = \frac{n_F[\epsilon_{\sigma}(\mathbf{k})] - n_F[\epsilon_{-\sigma}(\mathbf{k})]}{\epsilon_{-\sigma}(\mathbf{k}) - \epsilon_{\sigma}(\mathbf{k})}, \quad (10)$$

where  $n_F$  is the Fermi distribution function. In this case, the coefficient  $C_{\sigma - \sigma}$  is equal to  $K_{\sigma - \sigma}(Q)/[8\pi^3 K_{\sigma - \sigma}(0)]$ . As a result, the spin-non-diagonal local interaction is given by the form

$$\widetilde{W}_{\sigma - \sigma} = \frac{\int d\mathbf{k} d\mathbf{p} \gamma_{\sigma - \sigma}(\mathbf{k}) W(\mathbf{k} - \mathbf{p}, 0) \gamma_{\sigma - \sigma}(\mathbf{p})}{[8\pi^3 K_{\sigma - \sigma}(0)]^2}. \quad (11)$$

For the HEG in the spin-polarized state, we can rewrite Eq. (11) in the following way

$$\begin{aligned} \widetilde{W}_{\sigma - \sigma} &= \frac{1}{(4\pi)^2} \int d\Omega_{\mathbf{k}} d\Omega_{\mathbf{p}} \frac{1}{[2\zeta k_F^3/3]^2} \\ &\times \int_{k_F^{\sigma}}^{k_F^{-\sigma}} |\mathbf{k}|^2 d|\mathbf{k}| \int_{k_F^{\sigma}}^{k_F^{-\sigma}} |\mathbf{p}|^2 d|\mathbf{p}| W(\mathbf{k} - \mathbf{p}, 0). \end{aligned} \quad (12)$$

Note that the ratio  $\gamma_{\sigma - \sigma}$  tends to the  $\delta$ -function at the  $\zeta \rightarrow 0$  limit (the paramagnetic state), and the spin-diagonal and spin-non-diagonal parts become equal. Since in this paper we are interested in paramagnetic systems, the local interaction with  $\zeta \neq 0$  remains to be examined elsewhere.

## C. Local-field factor

In paper I, by examining the irreducible polarizability exchange diagrams [Fig. 1(b)], we have shown that for paramagnetic systems the local electron-hole interaction  $\widetilde{W}$  can be identified with the local-field factor  $\mathcal{G}(Q)$  (or more precisely with its exchange part)

$$\mathcal{G}(Q) = \widetilde{W}(Q)/2v_c(\mathbf{Q}), \quad (13)$$

where  $\widetilde{W}(Q) = \frac{1}{2} \sum_{\sigma} \widetilde{W}_{\sigma\sigma}(Q)$ , and  $v_c(\mathbf{Q})$  is the bare Coulomb interaction. This exchange part is related to the first-order exchange diagram in the irreducible polarizability diagrammatic expansion [see Eqs. (4), (5) and Figs. 1(b) and 1(d)]. Such a relation was derived and examined by many authors within various approaches (see, e.g., Refs. 21,24,25, and 31,32,33,34). Thus we can verify the approximation done for  $\widetilde{W}$  in the previous subsection.

Actually, at the considered limit ( $Q \rightarrow 0$ ), the local-field factor of the HEG has the form

$$\mathcal{G}(Q) = A \left( \frac{\mathbf{Q}}{k_F} \right)^2, \quad (14)$$

where  $A = \frac{\widetilde{W} k_F^2}{8\pi}$  in our case. This relation allows us to carry out, by the example of the HEG in the paramagnetic state, a comparison of the coefficient  $A$  obtained with the help of Eq. (9) with that known from the literature.

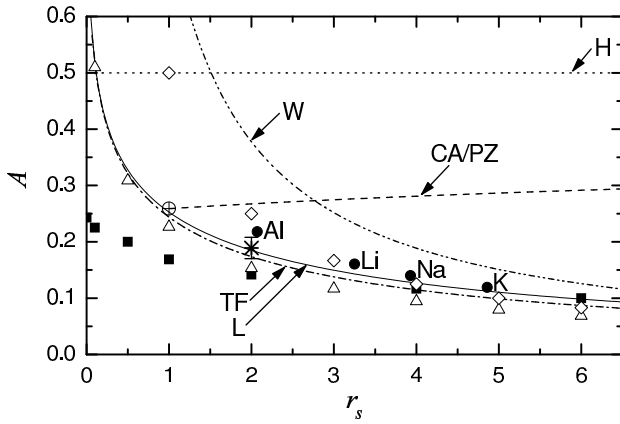


FIG. 2: The coefficient  $A$  versus the electron density parameter  $r_s$ . Filled squares and circles represent the results of Refs. 22 and 23, respectively. Stars with the error bar depict  $A$  obtained from calculations of  $\mathcal{G}_a$  for  $r_s = 2$  shown in Fig. 3 of Ref. 21. The notations H, CA/PZ, TF, L, and W signify, respectively, the Hubbard approximation, the results of Monte Carlo calculations of Ref. 36 ( $r_s \geq 1$ ), the Thomas-Fermi model [Eq. (15)], calculations by means of Eq. (9) with the use of the Lindhard function, and, finally,  $A$  obtained from Eq. (16). Open triangles and diamonds depict the “self-consistent” calculations (see the text) for the TF and W cases, respectively.

The simplest way to analytically perform the integration in Eq. (9) is to use the screened Coulomb interaction  $W(\mathbf{k}, 0) = 4\pi [|\mathbf{k}|^2 + q_{TF}^2]^{-1}$  of the Thomas-Fermi model (see, e.g., Ref. 35). Here  $q_{TF} = (\frac{4\alpha r_s}{\pi})^{1/2} k_F$  is the Thomas-Fermi wave vector, the electron density parameter  $r_s$  is given by  $\frac{4\pi}{3}(a_0 r_s)^3 = 1/n$ ,  $a_0$  being the Bohr radius,  $\alpha = (\frac{4}{9\pi})^{1/3}$ , and  $\alpha r_s k_F = 1$ . As a result, for  $A$  we obtain the following dependence on the electron density parameter:

$$A_{TF}(r_s) = \frac{1}{8} \ln \left( 1 + \frac{\pi}{\alpha r_s} \right). \quad (15)$$

In Fig. 2, we show  $A_{TF}$  as a function of  $r_s$  as well as the coefficient  $A_L$  (the “L” curve) calculated by means of Eqs. (9), (13), and (14) with the use of the Lindhard dielectric function. It follows from the figure that  $A_{TF}$  and  $A_L$  are very close to each other, especially at  $r_s \rightarrow 0$ . Moreover, both these results are in good agreement with the coefficient  $A$  obtained in Ref. 23 (in the figure it is shown for Al, Li, Na, and K), where the same class of ladder diagrams in the irreducible polarizability diagrammatic expansion was considered.

Also, as shown in Fig. 2, our results are in accord with calculations performed in Ref. 21 for the local-field factor  $\mathcal{G}_a$  [see Eq. (36) in the cited paper] which is formally the same as that of Eq. (13), except for including self-energy effects and the fact that  $\mathcal{G}_a$  is given on the imaginary-frequency axis. The shown error bar is originated from the procedure of evaluating of  $A$ : inspecting Fig. 3 of Ref. 21, we have found  $A$  from a set of values of  $\mathcal{G}_a$

evaluated at various momenta ( $0.4k_F$ ,  $0.6k_F$ ,  $0.8k_F$ , and  $1.0k_F$ ).

Due to the integration over the Fermi surface in Eq. (9), at the low-density limit ( $r_s \rightarrow \infty$ ), when the ratio  $q_{TF}/k_F$  is large, one can neglect momentum dependence of the screened Coulomb interaction. This leads to  $\bar{W} = W(0, 0)$  and, as a consequence,

$$A_W(r_s) = \frac{\pi}{8\alpha r_s}. \quad (16)$$

It is appropriate to mention here that the approximation made in Ref. 17 corresponds to the local interaction given by  $\widetilde{W}(Q) = W(\mathbf{Q}, 0)$ . This means that the local-field factor of Eq. (13) can be represented as

$$\mathcal{G}(\mathbf{Q}, 0) = \frac{1}{2\varepsilon(\mathbf{Q}, 0)}. \quad (17)$$

For the HEG, the approximation (17) gives a Hubbard-like form for  $\mathcal{G}$  and at the small four-momentum transfer limit it leads to  $A = A_W$ . Such an approximation can be valid at the low-density limit, whereas for  $r_s \lesssim 2.5$  it essentially overestimates the exchange diagrams contribution, exceeding even the accurate results of Monte Carlo calculations<sup>36</sup> which include both exchange and correlation effects (see Fig. 2).

It is worth pointing out that the common property of  $A_{TF}$ ,  $A_L$ , and  $A_W$  is the divergence at  $r_s \rightarrow 0$ .<sup>37</sup> In this connection, it makes sense to compare our results with the exchange local-field factor of Ref. 22 (filled squares in Fig. 2). A class of diagrams considered there comprises ladder diagrams based on more complex electron-hole interaction containing electron-electron and hole-hole multiple-scattering events. As a result, the coefficient  $A$  of Ref. 22 (evaluated from the local-field factor at  $k_F$  shown in Fig. 7 of the quoted paper) has no divergence in its dependence on  $r_s$ , tending to the Hartree-Fock prediction  $1/4$  at  $r_s \rightarrow 0$ . Nevertheless, by inspecting Fig. 2, we can infer that for the entire metallic density range ( $r_s$  from 2 to 6) even the simplest approximation  $A_{TF}$  yields results consistent with those known from the literature. This fact allows us to expect that the local electron-hole interaction (7)–(9) will give reasonable results on the self-energy ladder diagrams treatment.

At last, we would like to note that in order to more precisely evaluate the exchange part of  $\mathcal{G}$  from Eqs. (9) and (13), one can include the corresponding local-field corrections into  $W$  and perform a kind of “self-consistent” (sc) procedure.<sup>38</sup> As shown in Fig. 2 (open triangles and diamonds), such a procedure modifies  $A_{TF}$  slightly, whereas in the case of  $A_W$  the changes are more significant and the resultant  $A_{W:sc} = \frac{2}{3}A_W$  allows one to reasonably estimate the considered diagrams contribution in the entire metallic density range.<sup>39</sup> Moreover, the use of this prefactor  $2/3$  together with the approximation (17) in *ab initio* calculations<sup>40</sup> brings theory and experiment to a better agreement.

### III. QUASIPARTICLE PROPERTIES

In this section, we address the question of how the electron-hole multiple scattering affects quasiparticle properties which are determined by both the self-energy and its derivatives with respect to momentum and frequency. We study the HEG in the paramagnetic state at different values of  $r_s$  ranging from 2 to 56. This study includes the metallic density range ( $2 \lesssim r_s \lesssim 6$ ) as well as the range of large  $r_s \sim 48$  for which the effective mass “divergence” was predicted in Ref. 42.

#### A. Quasiparticle self-energy

In paper I, we have shown that the  $T$  matrix (1) allows one to go beyond the GWA by summing an infinite number of the electron-hole ladder diagrams shown in Fig. 1(c). In this case, the quasiparticle self-energy can be expressed as  $\Sigma_\sigma = \Sigma_\sigma^{GW} + \Sigma_\sigma^T$ , where the  $GW$  term is well known to be

$$\Sigma_\sigma^{GW}(p) = \frac{i}{(2\pi)^4} \int dk G_\sigma(k) W(p - k), \quad (18)$$

and the  $T$ -matrix contribution is given by

$$\Sigma_\sigma^T(p) = -\frac{i}{(2\pi)^4} \sum_{\sigma'} \int dk G_{\sigma'}(k) \mathcal{T}_{\sigma\sigma'}(p - k) \quad (19)$$

with  $\mathcal{T}_{\sigma\sigma'}(k) = \tilde{\Gamma}_{\sigma\sigma'}(k)[K_{\sigma\sigma'}(k)\tilde{W}_{\sigma\sigma'}(k)]^2$ . It is important that the  $T$ -matrix contribution (19) has a  $GW$ -like form that simplifies calculations of  $\Sigma_\sigma^T$ .

Due to the correspondence between multiple-scattering events and a spin fluctuation (see, e.g., Refs. 44 and 17,43,45,46,47,48), this approach to the self-energy includes the contributions of both charge and spin fluctuations. As a result, in such an approach, having retained all the advantages of the  $GW$  approximation, we have a possibility of describing quasiparticle properties more comprehensively than it can be done in the GWA. Note that as in the case of the irreducible polarizability ladder diagrams, the local interaction  $\tilde{W}_{\sigma\sigma'}$  is an object of principal concern here because  $\mathcal{T}_{\sigma\sigma'}$  depends significantly on the form for this interaction and, consequently, care must be taken by choosing an approximation to it.

In this work, we mainly focus our attention on the effect of the inclusion of the self-energy ladder diagrams on the quasiparticle properties in the case of the HEG in the paramagnetic state. For simplicity, we evaluate the  $GW$  term with the noninteracting Green function and the RPA screened interaction (the so-called  $G_0W_0$  approximation which gives a better description of the quasiparticle properties than the fully self-consistent  $GW$  approximation itself, except for the total energy<sup>41,49</sup>). Below, unless stated otherwise, this  $G_0W_0$  approximation is referred to as the GWA. To evaluate the  $T$ -matrix contribution, we also use the noninteracting Green function,

the RPA electron-hole propagator, and the local interaction elaborated in the previous section (corresponding to  $A_L$ ).

For the computational purposes, it is convenient to split up the  $GW$  term into the energy-independent Hartree-Fock (exchange) part  $\Sigma^{HF}(\mathbf{k})$  and the correlation part  $\Sigma_c^{GW}(\mathbf{k}, \omega)$  defined through Eq. (18) by the induced potential  $W_i = W - v_c$  instead of the screened interaction  $W$ . Within the spectral function representation,<sup>6</sup> having found the imaginary part of  $\Sigma_c^{GW}$  we obtain its real part,  $\text{Re}\Sigma_c^{GW}(\mathbf{k}, \omega)$ , from the Hilbert transform by using the principal value integration. As a result, the real part of the self energy in the GWA is equal to  $\text{Re}\Sigma^{GW}(\mathbf{k}, \omega) = \Sigma^{HF}(\mathbf{k}) + \text{Re}\Sigma_c^{GW}(\mathbf{k}, \omega)$ . Regarding the  $T$ -matrix contribution, we first evaluate  $\text{Im}\Sigma^T$  of Eq. (19) and then perform the Hilbert transform.

In order to get some idea of the quantity and behavior of the  $T$ -matrix contribution in comparison with the  $GW$  term, in Fig. 3 we plot the correlation part of the self-energy  $\Sigma_c^{GW}$  and the  $T$ -matrix contribution  $\Sigma^T$  as a function of the momentum and energy for  $r_s = 4$ . As follows from the figure, due to plasmon singularities of the inverse dielectric function, the  $GW$  term seems substantially larger than the  $T$ -matrix contribution.<sup>50</sup> However, inspecting Figs. 3(c) and 3(d), one can see that the  $\Sigma^T$  surface becomes notably corrugated in the vicinity of the  $\omega = 0$  energy where  $\Sigma^{GW}$  behaves smoothly and contains only the electron-hole contribution (the plasmon decay channel is not open yet in this energy range) which is comparatively not large. As a consequence, the  $T$ -matrix inclusion is expected to appreciably influence the quasiparticle properties (especially on those determined by the self-energy derivatives) in this energy region.

As is evident from Fig. 3(c), at some energies  $\omega < 0$  the spectral function of the  $T$ -matrix contribution becomes negative. However, it does not lead to wrong analytical properties of the self-energy, because the contribution (19) has such a form as an additional term beyond the  $GW$  one and, consequently, should be considered in sum with the latter. This sum is always non-negative.

Now we consider the on-shell imaginary part of the self-energy which gives the quasiparticle damping rate. In Fig. 4, we show this quantity as a function of momentum  $|\mathbf{k}|/k_F$  for  $r_s = 2$  and 4. First of all, we would like to note that despite the fact that the spectral function of  $\Sigma^T(\mathbf{k}, \omega)$  is negative within some  $\mathbf{k} - \omega$  domain the on-shell imaginary part of the  $T$ -matrix contribution has the same sign as the  $GW$  term at any value of momentum. This means that the  $T$ -matrix inclusion leads to an increase of the quasiparticle damping rate with respect to that in the GWA. In order to assess the quantity of this increase, we examine the ratio  $\text{Im}\Sigma/\text{Im}\Sigma^{GW} = 1 + \text{Im}\Sigma^T/\text{Im}\Sigma^{GW}$  (see inset of Fig. 4). According to the calculations performed, this ratio as a function of momentum has the largest value at  $|\mathbf{k}| \sim k_F$  and falls down when  $|\mathbf{k}|$  moves away from  $k_F$ . Furthermore, the lower the electron density that the HEG possesses, the larger the ratio we have. For example,

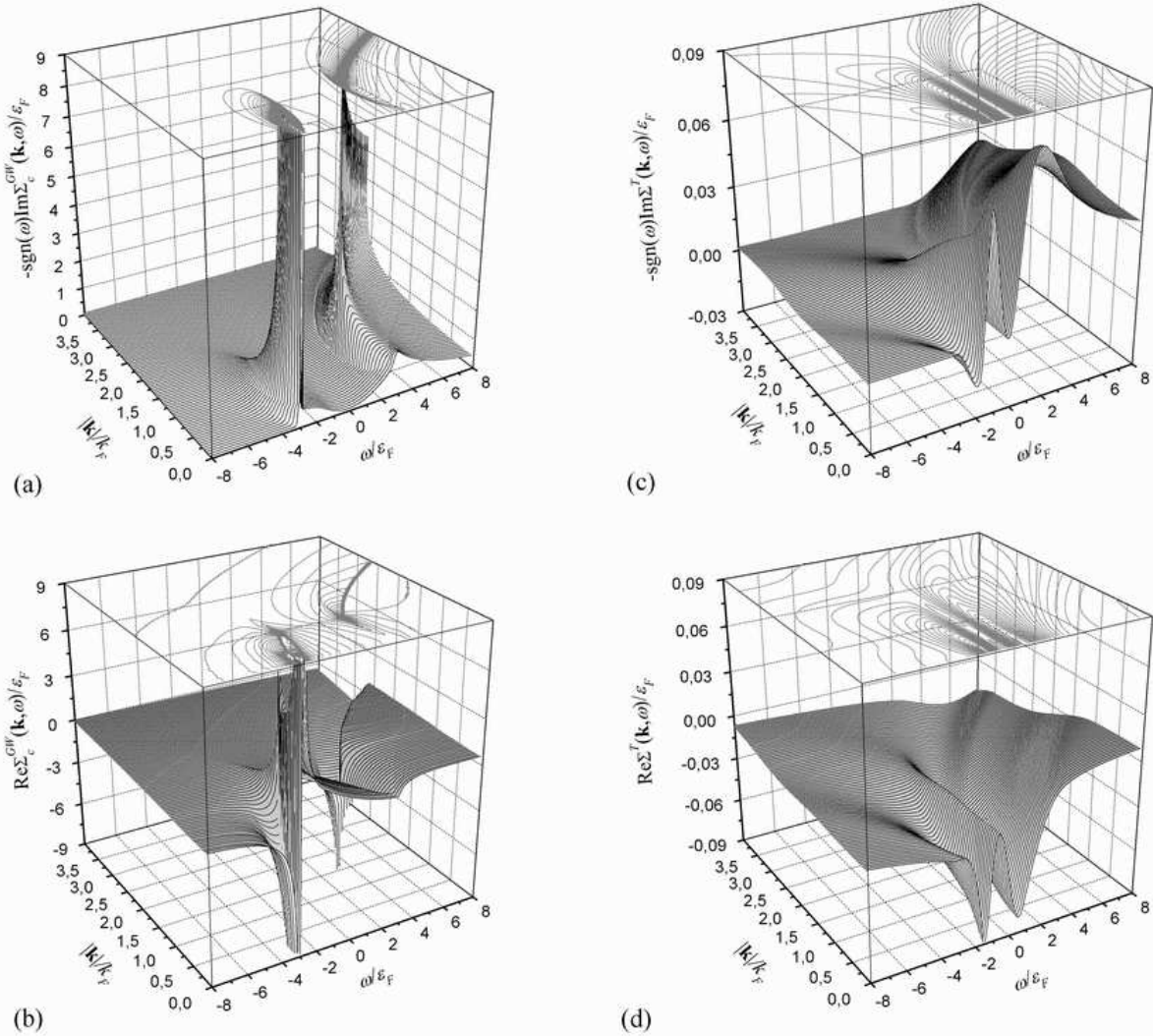


FIG. 3: The spectral function  $-\text{sgn}(\omega)\text{Im}\Sigma_c^{GW}$  (a) and the real part  $\text{Re}\Sigma_c^{GW}$  (b) of the correlation part of the self-energy calculated within the GWA. Also the spectral function  $-\text{sgn}(\omega)\text{Im}\Sigma^T$  (c) and the real part  $\text{Re}\Sigma^T$  (d) of the  $T$ -matrix contribution to the self-energy. The GWA self-energy and the  $T$ -matrix contribution are plotted as functions of energy  $\omega/\epsilon_F$  and momentum  $|\mathbf{k}|/k_F$  for  $r_s = 4$ . At the top of each of these figures, the contour plot (50 levels) is shown.

$\text{Im}\Sigma/\text{Im}\Sigma^{GW}$  evaluated at  $|\mathbf{k}| = 1.05k_F$  is equal to 1.33 for  $r_s = 2$  and 1.72 for  $r_s = 4$ .

As compared with the generalized  $GW$  self-energy evaluated in Ref. 41, for  $|\mathbf{k}| < k_F$  we have similar results which are very close quantitatively. However, it is not so for  $|\mathbf{k}| > k_F$  especially in the region where a quasiparticle can decay into plasmons. Under this region the on-shell imaginary part of the generalized  $GW$  self-energy very quickly becomes smaller than that in the GWA and then demonstrates a partial “suppression” of the plasmon decay channel in comparison with the  $GW$  approximation (see also Ref. 51).

Next, to answer the question of how the value of the ratio  $\text{Im}\Sigma/\text{Im}\Sigma^{GW}$  depends on the chosen form of the approximation for the local electron-hole interaction, we have calculated  $\text{Im}\Sigma^T$  with  $\widetilde{W}$  defined by Eq. (13) with the local-field factor (17) for  $r_s = 2$ . As follows from the

inset of Fig. 4, the ratio becomes essentially larger than that presented by dashed line and runs up to 2.53 at  $|\mathbf{k}| = 1.05k_F$ . This means that the use of such an interaction  $\widetilde{W}$  instead of Eq. (9) leads to an increase of the ratio by a factor of 1.90 at this momentum. Thus, keeping in mind that at the small four-momentum transfer limit this local interaction corresponds to the coefficient  $A_W$  of Eq. (16), we suppose that at least for aluminum the use of this approximation to  $\widetilde{W}$  results in a large value of the  $T$  matrix that in turn rises the quasiparticle damping rate too high. In connection with the coefficients shown in Fig. 2, we would like to note that, e.g., for  $r_s = 2$  the local-field factor of Ref. 23 used in paper I gives the increase of the ratio by a factor of 1.24.

Regarding the on-shell real part of the self-energy (see Fig. 5), we would like to emphasize that again the  $T$ -matrix contribution has the same sign as the  $GW$  term.

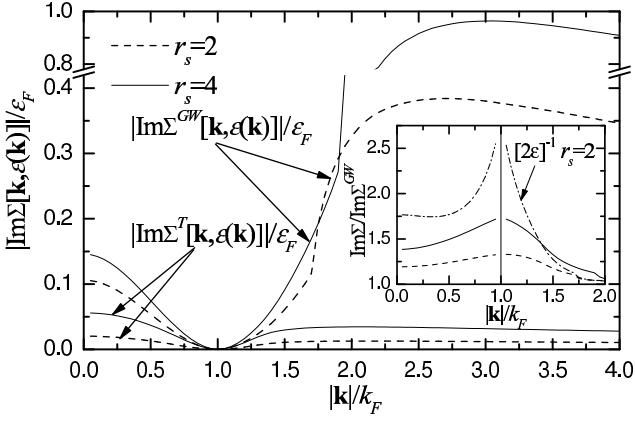


FIG. 4: The absolute value of the imaginary part of the self-energy evaluated at  $\omega = \epsilon(\mathbf{k})$  (the  $GW$  term and the  $T$ -matrix contribution) as a function of momentum  $|\mathbf{k}|/k_F$  for  $r_s = 2$  (dashed line) and  $4$  (solid line). Inset: the ratio  $\text{Im}\Sigma/\text{Im}\Sigma^{GW} = 1 + \text{Im}\Sigma^T/\text{Im}\Sigma^{GW}$  as a function of momentum  $|\mathbf{k}|/k_F$  for  $r_s = 2$  and  $4$ . The dash-dotted line represents this ratio evaluated with the local-field factor of Eq. (17) for  $r_s = 2$ .

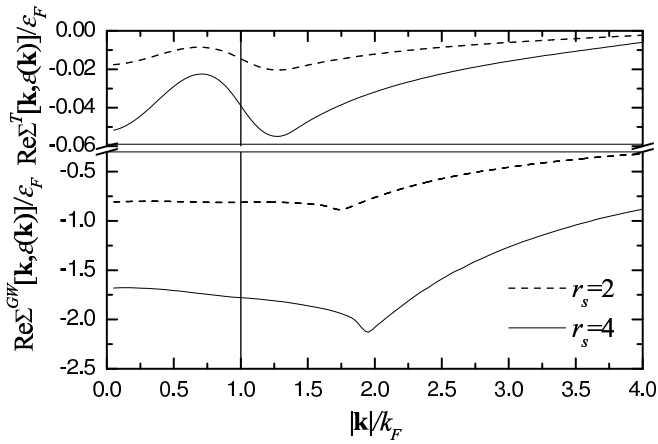


FIG. 5: The real part of the self-energy  $\text{Re}\Sigma[|\mathbf{k}|, \epsilon(\mathbf{k})]$  (the  $GW$  term and the  $T$ -matrix contribution) as a function of momentum  $|\mathbf{k}|/k_F$  for  $r_s = 2$  (dashed line) and  $r_s = 4$  (solid line).

Owing to the “corrugations” discussed in connection with Fig. 3, in the vicinity of  $k_F$   $\text{Re}\Sigma^T$  shows fast variation which for  $0.7k_F \lesssim |\mathbf{k}| \lesssim 1.3k_F$  can be fitted rather well by a sinelike function. As follows from Fig. 5, the  $T$ -matrix contribution represents itself as a very small quantity within all the considered  $\mathbf{k}$ -domain and therefore can alter the on-shell real part of the self-energy evaluated in the GWA to only a small extent.

In Figs. 6 and 7, we show how the  $GW$  term and the  $T$ -matrix contribution depend on  $r_s$  beyond the metallic density range. One can see that the on-shell  $\text{Im}\Sigma^{GW}$  as a function of  $r_s$  shows relatively small changes for  $0.0k_F \leq |\mathbf{k}| \lesssim 1.5k_F$  and already at  $r_s \sim 24$  gets some “saturation”, whereupon properties of the  $e - h$

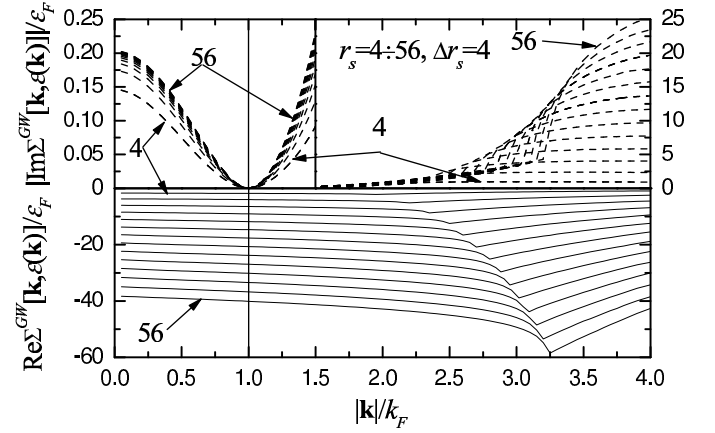


FIG. 6: The on-shell real and imaginary parts of the self-energy calculated in the GWA as functions of momentum  $|\mathbf{k}|/k_F$  for  $r_s$  values ranging from  $4$  to  $56$ .

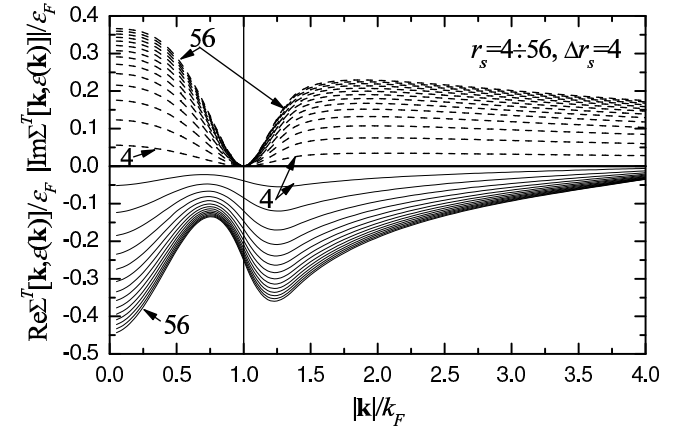


FIG. 7: The on-shell real and imaginary parts of the  $T$ -matrix contribution as functions of momentum  $|\mathbf{k}|/k_F$  for  $r_s$  values ranging from  $4$  to  $56$ .

decay channel remain practically unchanged within the mentioned  $\mathbf{k}$  interval. For  $|\mathbf{k}| > 1.5k_F$ , especially in the plasmon emission region, the quasiparticle damping rate demonstrates a continual increase with increasing  $r_s$ . Owing to this and the  $r_s$ -dependence of  $\Sigma^{HF}$ , the on-shell real part of the  $GW$  self-energy monotonically decreases as a function of  $r_s$ . As to the  $T$ -matrix contribution, after  $r_s \sim 40$  the changes of the imaginary and real parts become insignificant for any momentum.<sup>52</sup>

In Fig. 8, we plot the ratio  $\text{Im}\Sigma/\text{Im}\Sigma^{GW}$  as a function of  $r_s$  evaluated for different momenta. In fact this figure shows how the inclusion of the self-energy ladder diagrams affects the quasiparticle damping rate. The biggest contribution of these diagrams is observed in the vicinity of  $k_F$  and can exceed the GWA prediction, e.g., by a factor of 3.6 at  $r_s = 56$ .

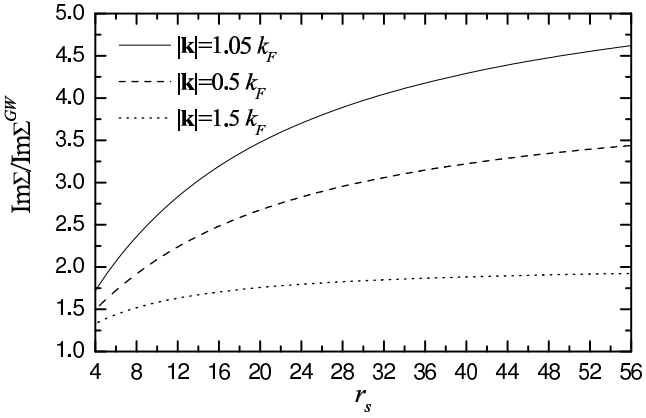


FIG. 8: The ratio  $\text{Im}\Sigma/\text{Im}\Sigma^{\text{GW}} = 1 + \text{Im}\Sigma^T/\text{Im}\Sigma^{\text{GW}}$  as a function of  $r_s$  at  $|\mathbf{k}| = 0.5k_F$  (dashed line),  $1.05k_F$  (solid line), and  $1.5k_F$  (dotted line).

### B. Quasiparticle energy, renormalization constant, and effective mass enhancement

The quasiparticle excitation energy within the first-order perturbation theory is given by

$$E_k = \epsilon(\mathbf{k}) + \text{Re}\Sigma[\mathbf{k}, \epsilon(\mathbf{k})] - \text{Re}\Sigma[k_F, 0], \quad (20)$$

where the real part of the self-energy in the on-shell approximation is added to the single-particle energy. In Fig. 9, we show the calculated  $E_k$  for  $r_s = 2$  and 4. Due to the small value of the on-shell real part of the  $T$ -matrix contribution, the quasiparticle dispersion is only slightly changed by the inclusion of the self-energy ladder diagrams. Inspecting the figure, one can see that this inclusion results in a light increase of the bandwidth with respect to the  $GW$  one. This increase is similar to that evaluated in Ref. 10 within the  $GW\Lambda$  approximation with the inclusion of the same vertex function in the screened interaction and the numerator of the self-energy. However this similarity is observed only under  $r_s \sim 4$ . For  $r_s \gtrsim 4$ , the  $GW\Lambda$  approximation yields band narrowing greater than the GWA does.

As was anticipated, we have a more profound effect of the  $T$ -matrix inclusion on the quasiparticle properties determined by the derivatives of the self-energy. One of such properties is the effective mass enhancement which in the on-shell approximation is known to be given by

$$\frac{m^*(\mathbf{k})}{m} = \left[ \frac{m}{k} \frac{dE_k}{dk} \right]^{-1}. \quad (21)$$

The inset of Fig. 9 represents the inverse value of this dispersing quasiparticle effective mass for  $r_s = 2$  and 4. A close examination of  $m/m^*$  as a function of momentum provides interesting insights. First, owing to the sinelike behavior of the on-shell  $\text{Re}\Sigma^T$  in the vicinity of  $k_F$  (see Fig. 5), the  $T$ -matrix inclusion gives alternating contribution to the inverse effective mass. As a result,  $m/m^*$  becomes smaller at  $|\mathbf{k}| \sim k_F$  and greater away from it.

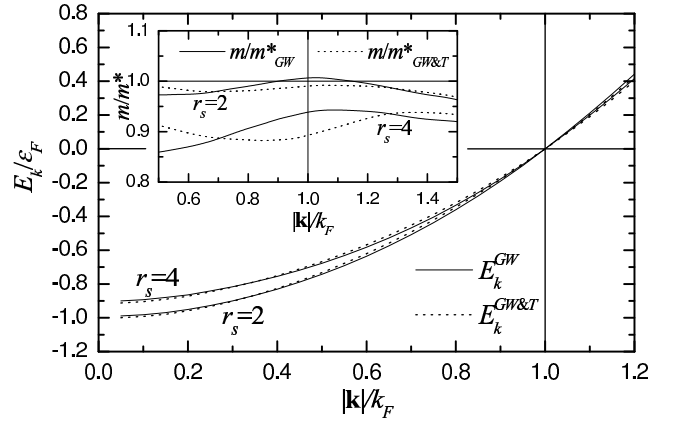


FIG. 9: The quasiparticle energy  $E_k$ , Eq. (20), calculated without ( $GW$ , solid line) and with ( $GW\&T$ , dotted line) the  $T$ -matrix contribution as a function of momentum  $|\mathbf{k}|/k_F$  for  $r_s = 2$  and  $r_s = 4$ . Inset: the inverse effective mass enhancement  $m/m^*$  as a function of  $|\mathbf{k}|/k_F$  for  $r_s = 2$  and 4.

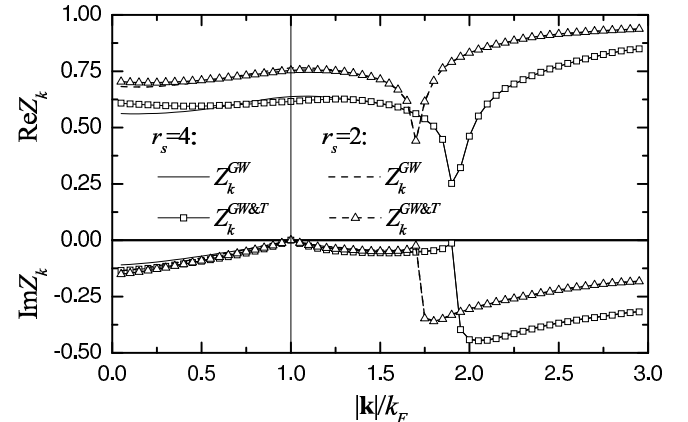


FIG. 10: The real and imaginary parts of the renormalization constant  $Z_k$  calculated without ( $GW$ ) and with ( $GW\&T$ ) the  $T$ -matrix contribution as a function of momentum  $|\mathbf{k}|/k_F$  for  $r_s = 2$  and 4.

At some momenta the  $T$ -matrix contribution to the effective mass is equal to zero. Second, for  $r_s = 2$  multiple electron-hole scattering modifies the effective mass to an extent that quasiparticles become “heavier” than in the noninteracting system, whereas the GWA predicts the reverse. Third, as can be seen from Fig. 5, for  $r_s = 4$  the absolute value of the derivative of the on-shell  $\text{Re}\Sigma^T$  with respect to momentum should be larger than that for  $r_s = 2$ . This entails the larger alteration of  $m/m^*$ . Thus, focusing our attention on the effective mass behavior in the vicinity of  $k_F$ , we can infer that the multiple electron-hole scattering leads to a “weighting” of quasiparticles.

Note that Eq. (21) is a valid approximation to the effective mass enhancement at small values of  $r_s$ .<sup>41</sup> In order to estimate the quasiparticle effective mass at  $k_F$  more precisely, especially for large  $r_s$ , we use the formally exact

TABLE I: The effective mass enhancement  $m^*/m$  and the renormalization constant  $Z_F$  at the Fermi wave vector  $k_F$  calculated without ( $GW$ ) and with ( $GW\&T$ ) the  $T$ -matrix contribution. In each of these cases, two values of the mass enhancement are presented: the first one is obtained from the exact formula, Eq. (22), the second one (in parentheses) is calculated within the on-shell approximation, Eq. (21).

$r_s$	$m^*/m$		$Z_F$	
	$GW$	$GW\&T$	$GW$	$GW\&T$
2	0.99 (0.99)	1.01 (1.01)	0.77	0.75
4	1.05 (1.07)	1.08 (1.12)	0.64	0.62

equation<sup>35</sup>

$$\frac{m^*}{m} = \frac{Z_F^{-1}}{1 + \frac{m}{k_F} \frac{\partial \Sigma(\mathbf{k}, \omega)}{\partial k} \Big|_{\omega=0, |\mathbf{k}|=k_F}}. \quad (22)$$

Here  $Z_F$  is the renormalization constant  $Z_k$  evaluated at the Fermi wave vector. In its turn, the renormalization constant  $Z_k$  that gives the spectral weight of the quasi-particle is defined for a four-momentum  $[\mathbf{k}, \epsilon(\mathbf{k})]$  as<sup>35</sup>

$$Z_k = \left[ 1 - \frac{\partial \Sigma(\mathbf{k}, \omega)}{\partial \omega} \Big|_{\omega=\epsilon(\mathbf{k})} \right]^{-1}. \quad (23)$$

In Fig. 10, we plot the renormalization constant as a function of momentum for  $r_s = 2$  and 4. It follows from the figure that changes of the real part of  $Z_k$  caused by the  $T$ -matrix inclusion occur mainly up to  $|\mathbf{k}| \sim 1.5k_F$ . The imaginary part of  $Z_k$  accounting for multiple electron-hole scattering differs weakly from that in the GWA. At  $|\mathbf{k}| = k_F$ , the renormalization constant is real. Due to the fact that the frequency derivative  $\frac{\partial \text{Re}\Sigma^T}{\partial \omega} \Big|_{|\mathbf{k}|=k_F, \omega=0}$  is negative as well as in the case of the

$GW$  term (see Fig. 3),  $Z_F$  becomes smaller with the  $T$ -matrix inclusion. Together with the positive momentum derivative of  $\text{Re}\Sigma^T$  it affects the effective mass of Eq. (22) and moves the latter away from its value obtained in the GWA. Table I contains our detailed results on the effective mass enhancement and the renormalization constant for  $r_s = 2$  and 4.

In Fig. 11, we show the calculated dependence of  $Z_F$  and  $m/m^*$  on  $r_s$  and compare it with that known from the literature. As follows from Fig. 11(a), the inclusion of the  $T$  matrix reduces the renormalization constant  $Z_F$ . Thereby the  $T$ -matrix contribution shifts the  $Z_F$ -curve towards the so-called GZ (Gori-Giorgi-Ziesche) parametrization of Ref. 57. This parametrization is in good agreement with calculations of Ref. 54 performed by making use of the effective-potential-expansion (EPX) method which in contrast to the Hedin expansion<sup>5</sup> is formulated in terms of the static screened interaction  $W(\mathbf{q}, 0)$ . The GZ parametrization is also compatible with QMC data found in Ref. 55 for the HEG momentum distribution. The fact that the renormalization constant  $Z_F$

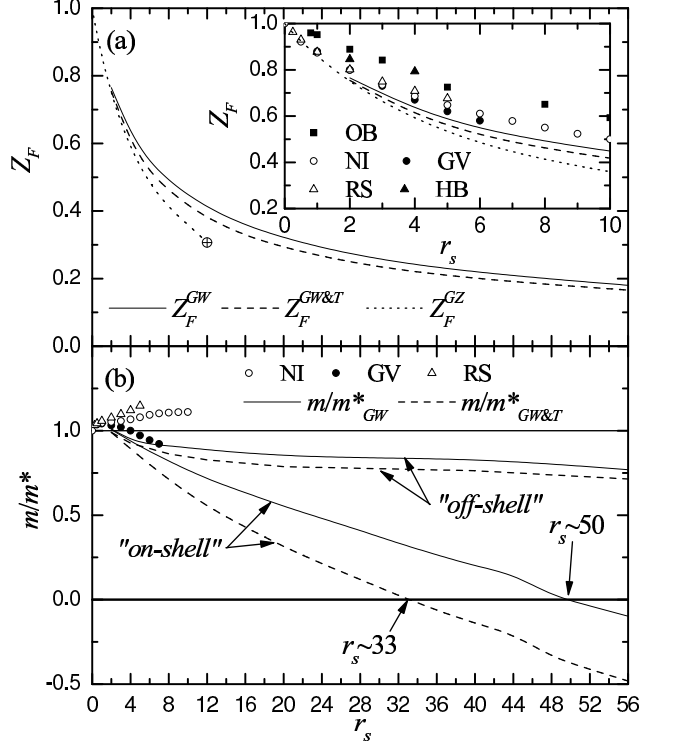


FIG. 11: (a) The renormalization constant  $Z_F$  at the Fermi wave vector obtained without ( $GW$ , solid line) and with ( $GW\&T$ , dashed line) the  $T$ -matrix contribution as a function of  $r_s$ . The dotted line represents the so-called GZ parametrization (Ref. 57) which is valid in the density range  $r_s \lesssim 12$ . The inset shows the obtained results in comparison with those known from the literature. (b) The inverse effective mass enhancement  $m/m^*$  at the Fermi wave vector calculated both in the on-shell approximation, Eq. (21), labeled as “on-shell”, and by making use of the formally exact Dyson equation (22), labeled as “off-shell”. The notations OB, NI, GV, RS, and HB signify the correspondent values taken from Refs. 55, 53, 41, 56, and 49, respectively.

determined by Monte Carlo<sup>55</sup> (labeled as OB in the figure) is noticeably larger than the parametrization can be explained by the difference in procedures of finding the momentum distribution discontinuity at  $k_F$ . In the QMC calculations there is a finite distance between momenta (including the closest to  $k_F$ ) for which the momentum distribution is calculated (see, e.g., Fig. 12 in Ref. 55), whereas the GZ parametrization allows one to find  $Z_F$  from  $|\mathbf{k}| \rightarrow k_F \pm 0$  limits.

Note that the self-consistent schemes of Refs. 49 (HB), 53 (NI), and 56 (RS), exhibit an increase of the quasi-particle renormalization constant at the Fermi surface with respect to  $Z_F^{GW}$  shown in Fig. 11(a). It can be understood within the framework of the detailed analysis carried out in Ref. 49, where the self-consistency between the Green function and the self-energy within the  $GW$  approximation has been achieved. As was shown,<sup>49</sup> the self-consistency procedure leads to the strongly suppressed plasmon peaks in the imaginary part of the self-

energy. Owing to the Hilbert transform, it entails an essential smoothing of the corresponding sharp structures of the self-energy real part. As a consequence, the frequency derivative of the latter, which is negative, becomes smaller by absolute value, that, in its turn, through Eq. (23) leads to an increase of the renormalization constant.

As regards the effective mass enhancement, it is evident from Fig. 11(b) that the on-shell approximation (21) underestimates  $m/m^*$  in comparison with that obtained from Eq. (22). At large values of  $r_s$  it comes into particular prominence. The on-shell  $GW$  effective mass exhibits a divergence at  $r_s \sim 50$  (in Ref. 42 at  $r_s \sim 48$ ). The  $T$ -matrix inclusion results in a considerable increase of the on-shell effective mass and leads to the divergence at  $r_s \sim 33$ . The effect of taking into account multiple electron-hole scattering on the effective mass calculated by making use of the formally exact equation (22) is consistent with the influence of the  $T$ -matrix inclusion on the renormalization constant. In this case the quasiparticle mass demonstrates a relatively weak  $r_s$  dependence without any divergence up to the largest  $r_s$  considered in the paper.

Regarding the  $r_s$  dependence of the quasiparticle effective mass, one can note that the effective mass is a more controversial quantity than the renormalization constant. Actually, comparing our  $m/m^*(r_s)$  with that of calculations of Refs. 56 ("RS") and 53 ("NI"), we find that contrary to our results the self-consistent schemes predict a monotonic increase of the inverse effective mass as a function of  $r_s$ . Such an increase is important to imply a bandwidth widening at metallic densities that disagrees with the experimental findings. Thus together with  $Z_F$  slightly "overestimated" in comparison with the GWA [see inset of Fig. 11(a)] these schemes yield the effective mass smaller than that in the noninteracting system, whereas the GWA gives the reverse. According to Eq. (22), it means that in the RS and NI cases the momentum derivative of the self-energy is larger than that evaluated in the GWA. Seemingly, it is caused by a large contribution of the Hartree-Fock part which is the self-energy for the noninteracting systems providing the effective mass equal to zero at the Fermi surface. This contribution cannot be canceled by the correlation part of the self-energy in full measure, as it occurs in the non-self-consistent GWA (see Ref. 49). As a result, this leads to an increase of the  $m/m^*$  ratio. To all appearances, at least for  $r_s < 4$  we have a similar situation in the generalized  $GW$  self-energy calculations of Ref. 41.

#### IV. CONCLUSIONS

In conclusion, we have presented a detailed study of the effect of multiple electron-hole scattering on quasiparticle properties determined by both the self-energy and its derivatives with respect to momentum and frequency. To take into account multiple scattering between an electron

and a hole in calculations of the self-energy  $\Sigma$ , a variational solution of the corresponding Bethe-Salpeter equation obtained in our preceding paper<sup>19</sup> has been used. This solution representing the  $T$  matrix within a local approximation allows one to sum the self-energy ladder diagrams. To preserve the advantages of the GWA, we have considered the sum of these diagrams as an additional term (the  $T$ -matrix contribution  $\Sigma^T$ ) to the  $GW$  self-energy  $\Sigma^{GW}$ . In this approach all weight of the problem is transferred to a form chosen for the local electron-hole interaction  $W$  that appears in the definition of the  $T$  matrix. By examining the irreducible polarizability ladder diagrams, one can identify this interaction with the exchange part of the many-body local-field factor. Considering this local interaction at the small four-momentum transfer limit, we have arrived at the expression which gives the results for the exchange local-field factor in accordance with those known from the literature.

Using the obtained form of  $\widetilde{W}$ , we have carried out extensive calculations of both the  $\Sigma^{GW}$  and  $\Sigma^T$  terms and such quasiparticle properties as the damping rate, the quasiparticle energy, the renormalization constant, and the effective mass enhancement over a broad range of electron densities in the homogeneous electron gas. The calculations have shown that the  $T$ -matrix inclusion leads to an increase of the quasiparticle damping rate especially in the vicinity of  $k_F$ . This increase depends on  $r_s$  and can exceed the  $GW$  prediction by a factor of 1.8 for  $r_s = 12$  and 3.6 for  $r_s = 56$ . Regarding the question of how a form chosen for the local interaction affects the quasiparticle damping rate, we have found that the latter is a very form-sensitive quantity, and consequently it is easy to over(under)estimate the ladder diagrams contribution. We have also revealed that due to small values of the on-shell real part of  $\Sigma^T$  the  $T$ -matrix inclusion modifies slightly the quasiparticle dispersion reducing the  $GW$  band narrowing.

We have found that the  $T$ -matrix contribution can notably affect the renormalization constant and the effective mass enhancement. Examining the renormalization constant  $Z_F$  as a function of  $r_s$  at the Fermi surface, we have ascertained that in comparison with the  $GW$  values the  $T$ -matrix inclusion reduces  $Z_F$ . As a result, the latter becomes closer to the renormalization constant given by the GZ parametrization<sup>57</sup> compatible with QMC calculations of the momentum distribution. A close analysis of the quasiparticle effective mass  $m^*/m$  evaluated both in the on-shell approximation and in the formally exact Dyson scheme (the off-shell approximation) has shown that the on-shell effective mass depends strongly on  $r_s$  and has a divergence<sup>42</sup> which is shifted by the  $T$ -matrix inclusion from  $r_s \sim 50$  (in the GWA) to  $r_s \sim 33$ . The off-shell  $m^*/m$  exhibits relatively weak  $r_s$  dependence and does not diverge up to the largest  $r_s$  considered. In this case, the  $T$ -matrix contribution leads only to a slight increase of "the weight of quasiparticles".

## Acknowledgments

We would like to thank N.W. Ashcroft and I. Nagy for useful discussions. The work was partially supported by the Research and Educational Center of Tomsk State

University, Departamento de Educación del Gobierno Vasco, MCyT (Grant No. FIS 2004-06490-C03-01), and by the European Community 6th framework Network of Excellence NANOQUANTA (Grant No. NMP4-CT-2004-500198).

---

<sup>\*</sup> Also at: Theoretical Physics Department, Kostroma State University, 156961 Kostroma, Russia.

<sup>1</sup> For a recent review, see W.G. Aulbur, L. Jönsson, and J. Wilkins, in *Solid State Physics*, edited by H. Ehrenreich and F. Saepen (Academic Press, New York, 2000), Vol. 54, p. 1.

<sup>2</sup> I. Campillo, V. M. Silkin, J. M. Pitarke, E. V. Chulkov, A. Rubio, and P. M. Echenique, Phys. Rev. B **61**, 13484 (2000).

<sup>3</sup> S.V. Faleev, M. van Schilfgaarde, and T. Kotani, Phys. Rev. Lett. **93**, 126406 (2004).

<sup>4</sup> V. P. Zhukov, F. Aryasetiawan, E. V. Chulkov, I. G. de Gurtubay, and P. M. Echenique, Phys. Rev. B **64**, 195122 (2001).

<sup>5</sup> L. Hedin, Phys. Rev. **139**, A796 (1965).

<sup>6</sup> F. Aryasetiawan in *Strong Coulomb Correlations in Electronic Structure Calculations*, edited by V.I. Anisimov (Gordon and Beach, Singapore, 2001).

<sup>7</sup> N.E. Zein and V.P. Antropov, Phys. Rev. Lett. **89**, 126402 (2002).

<sup>8</sup> S. Biermann, F. Aryasetiawan, and A. Georges, Phys. Rev. Lett. **90**, 086402 (2003).

<sup>9</sup> F. Aryasetiawan, M. Imada, A. Georges, G. Kotliar, S. Biermann, and A.I. Lichtenstein, Phys. Rev. B **70**, 195104 (2004).

<sup>10</sup> G.D. Mahan and B.E. Sernelius, Phys. Rev. Lett. **62**, 2718 (1989).

<sup>11</sup> I.G. Gurtubay, J.M. Pitarke, and P.M. Echenique, Phys. Rev. B **69**, 245106 (2004).

<sup>12</sup> G. Vignale and K.S. Singwi, Phys. Rev. B **32**, 2156 (1985); Tai Kai Ng and K.S. Singwi, *ibid.* **34**, 7738 (1986).

<sup>13</sup> C. A. Kukkonen and A.W. Overhauser, Phys. Rev. B **20**, 550 (1979).

<sup>14</sup> S. Yarlagadda and G. F. Giuliani, Phys. Rev. B **61**, 12556 (2000).

<sup>15</sup> I. Nagy, M. Alducin, and P. M. Echenique, Phys. Rev. B **65**, 235102 (2002).

<sup>16</sup> R. Asgari, B. Davoudi, M. Polini, G.F. Giuliani, M.P. Tosi, and G. Vignale, Phys. Rev. B **71**, 045323 (2005).

<sup>17</sup> V.P. Zhukov, E.V. Chulkov, and P.M. Echenique, Phys. Rev. Lett. **93**, 096401 (2004); V.P. Zhukov, O. Andreyev, D. Hoffman, M. Bauer, M. Aeschlimann, E.V. Chulkov, and P.M. Echenique, Phys. Rev. B **70**, 233106 (2004); V.P. Zhukov, E.V. Chulkov, and P.M. Echenique, *ibid.* **72**, 155109 (2005).

<sup>18</sup> J. Schäfer, M. Hoinkis, E. Rotenberg, P. Blaha, and R. Claessen, Phys. Rev. B **72**, 155115 (2005).

<sup>19</sup> I.A. Nechaev and E.V. Chulkov, Phys. Rev. B **71**, 115104 (2005).

<sup>20</sup> A.L. Fetter and J.D. Walecka, *Quantum Theory of Many-particle Systems* (McGraw-Hill, New York, 1971).

<sup>21</sup> C.F. Richardson and N.W. Ashcroft, Phys. Rev. B **50**, 8170 (1994).

<sup>22</sup> H. Suehiro, Y. Ousaka, and H. Yasuhara, J. Phys. C: Solid State Phys. **19**, 4247 (1986).

<sup>23</sup> A. Tsolakidis, E.L. Shirley, and R.M. Martin, Phys. Rev. B **69**, 035104 (2004).

<sup>24</sup> K. Sturm and A. Gusarov, Phys. Rev. B **62**, 16474 (2000).

<sup>25</sup> I.V. Tokatly and O. Pankratov, Phys. Rev. Lett. **86**, 2078 (2001).

<sup>26</sup> The RPA irreducible polarizability  $P^0(q) = -\sum_{\sigma} K_{\sigma\sigma}(q)$ .

<sup>27</sup> A.A. Abrikosov, L.P. Gor'kov, and I.E. Dzyaloshinski, *Methods of Quantum Field Theory in Statistical Physics* (Dover Publications, New York, 1963).

<sup>28</sup> At the Fermi surface, the density of states is assumed to be nonzero.

<sup>29</sup> The regular part  $\varphi$  is essential only in the integral over remote domain where the dynamically screened Coulomb interaction is weak.

<sup>30</sup> T. Moriya, *Spin Fluctuations in Itinerant Electron Magnetism* (Springer, Berlin, 1985).

<sup>31</sup> R. Stubner, I.V. Tokatly, and O. Pankratov, Phys. Rev. B **70**, 245119 (2004).

<sup>32</sup> G. Adragna, R. Del Sole, and A. Marini, Phys. Rev. B **68**, 165108 (2003).

<sup>33</sup> A. Marini, R. Del Sole, and A. Rubio, Phys. Rev. Lett. **91**, 256402 (2003).

<sup>34</sup> F. Bruneval, F. Sottile, V. Olevano, R. Del Sole, and L. Reining, Phys. Rev. Lett. **94**, 186402 (2005).

<sup>35</sup> G.D. Mahan, *Many-Particle Physics* (Plenum Press, New York, 1990).

<sup>36</sup> D.M. Ceperley and B.J. Alder, Phys. Rev. Lett. **45**, 566 (1980) as parametrized by J.P. Perdew and A. Zunger, Phys. Rev. B **23**, 5048 (1981).

<sup>37</sup> At that, due to the relation (14), the local-field factor and, consequently, the local interaction  $\tilde{W}$  go towards zero.

<sup>38</sup> We write “self-consistent” in quotation marks because it is not implied the full cycle of recalculations of the self-energy, the Green function, and so on.

<sup>39</sup> This prefactor of “self-consistency” is interesting to essentially bring the Hubbard approximation results closer to those evaluated from Monte Carlo calculations of Ref. 36.

<sup>40</sup> A. Mönnich, J. Lange, M. Bauer, M. Aeschlimann, I.A. Nechaev, V.P. Zhukov, P.M. Echenique, and E.V. Chulkov, cond-mat/0604067 (unpublished).

<sup>41</sup> G.F. Giuliani and G. Vignale, *Quantum Theory of the Electron Liquid* (Cambridge University Press, Cambridge, England, 2005).

<sup>42</sup> Y. Zhang and S. Das Sarma, Phys. Rev. B **71**, 045322 (2005); Y. Zhang, V.M. Yakovenko, and S. Das Sarma, *ibid.* **71**, 115105 (2005).

<sup>43</sup> D.J. Kim, Phys. Rev. B **37**, 7643 (1988).

<sup>44</sup> S. Doniach and S. Engelsberg, Phys. Rev. Lett. **17**, 750 (1966).

<sup>45</sup> W.F. Brinkman and S. Engelsberg, Phys. Rev. **169**, 417 (1968).

<sup>46</sup> J.A. Hertz and D.M. Edwards, Phys. Rev. Lett. **28**, 1334 (1972).

<sup>47</sup> P.S. Riseborough, Phys. Rev. B **27**, 5775 (1983).

<sup>48</sup> K. Karlsson and F. Aryasetiawan, Phys. Rev. B **62**, 3006 (2000); F. Aryasetiawan and K. Karlsson, *ibid.* **60**, 7419 (1999).

<sup>49</sup> U. von Barth and B. Holm, Phys. Rev. B **54**, 8411 (1996); B. Holm and U. von Barth, *ibid.* **57**, 2108 (1998).

<sup>50</sup> It is necessary to note that the picture may differ drastically in the case of the HEG in the spin-polarized state where magnon peaks appear in  $\text{Im}\Sigma^T$ .

<sup>51</sup> G.E. Santoro and G.F. Giuliani, Phys. Rev. B **39**, 12 818 (1989).

<sup>52</sup> Note that the coefficient  $A$  used does not meet the condition  $\frac{4\alpha r_s}{\pi}A = 1$  of a ferromagnetic instability.

<sup>53</sup> A. Nakano and S. Ichimaru, Phys. Rev. B **39**, 4930 (1989); **39**, 4938 (1989).

<sup>54</sup> Y. Takada, Phys. Rev. B **43**, 5979 (1991); Y. Takada and H. Yasuhara, *ibid.* **44**, 7879 (1991).

<sup>55</sup> G. Ortiz and P. Ballone, Phys. Rev. B **50**, 1391 (1994); **56**, 9970 (1997).

<sup>56</sup> H. Rietschel and L.J. Sham, Phys. Rev. B **28**, 5100 (1983).

<sup>57</sup> P. Gori-Giorgi and P. Ziesche, Phys. Rev. B **66**, 235116 (2002).